Reduction of End Effect–Induced Zone Broadening in Field–Flow Fractionation Channels

ARTICLE *in* ANALYTICAL CHEMISTRY · JANUARY 2007

Impact Factor: 5.64 · DOI: 10.1021/ac0610154 · Source: PubMed

3 AUTHORS, INCLUDING:

Himanshu Sant
University of Utah
41 PUBLICATIONS **146** CITATIONS

SEE PROFILE

Bruce K Gale
University of Utah
171 PUBLICATIONS **2,190** CITATIONS

SEE PROFILE

Anal. Chem. **2006,** *78,* 7978−7985

Reduction of End Effect-Induced Zone Broadening in Field-Flow Fractionation Channels

Himanshu J. Sant*

Center for Biomedical Microfluidics, Department of Bioengineering, University of Utah, 50 South Central Campus Drive, Room 2480, Salt Lake City, Utah 84112

Jung Woo Kim† and Bruce K. Gale‡

Center for Biomedical Microfluidics, Department of Mechanical Engineering, University of Utah, 50 South Central Campus Drive, Room 2110, Salt Lake City, Utah 84112

A channel configuration for the elimination of end effects in field-flow fractionation (FFF) channels is simulated and demonstrated for a microfabricated FFF system. In field-flow fractionation, the carrier liquid and sample particles are transferred from a point injection to the full breadth of the rectangular channel using a triangular end piece at the inlet. The nonuniformity in streamline length generated by this end piece results in an increased instrument-related plate height. An additional contribution from the end piece at the outlet of the channel further increases the total band broadening. This paper presents a novel approach to minimize end-effect contributions to plate height by fabricating microstructures in the channel end sections to redistribute the flow streams and force streamline lengths to be more uniform. Numerical analysis of the flow profile and sample dispersion (including spreading of particles due to diffusion and advection) is carried out to investigate the optimized microstructure column size, shape, and placement in the end pieces. The configuration obtained from the numerical simulation results is used to design a prototype device. Experimental measurement of the plate heights for this prototype with an on-chip impedance-based detector shows marked improvement in performance due to the presence of the microstructures in comparison to conventional FFF channel geometry with an average 50% reduction in plate height. The redesigned inlet triangle results in a uniform transition of the point-injected sample into a thin and straight band across the width of the channel at the start of the rectangular section of the fractionation channel.

Field-flow fractionation (FFF) is a flow-based chromatography technique that was invented by J. C. Giddings in 1966 at the University of Utah.[1] FFF-based systems consist of a long, thin, open channel that is sandwiched between two parallel plates that comprise the channel walls. The combination of an applied field in a direction perpendicular to the flow and the parabolic flow profile associated with laminar flow forces analytes in the separation channel to differential velocity zones in the channel, depending on their physiochemical properties, which induces separation. Because FFF does not require a stationary phase, FFF possesses certain unique advantages when compared to conventional chromatography, including an elution-based separation and open channel geometry that allows FFF to process delicate biological materials with minimal requirements for postprocessing, an ability to fractionate a wide size range of macromolecules in suspended and dissolved form, and the opportunity to tune the field type or flow conditions to maximize separation. The use of microfabrication technology and suitable packaging schemes has enhanced the performance of a variety of field-flow fractionation subtypes.[2−6] Still, there remains room for improvement in FFF instrument design to further enhance the system's efficiency.

In field-flow fractionation, analyte is typically injected at a point at the tip of the triangular end of the channel. This point-injected sample is transferred to the rectangular section, approximating infinite parallel plates through a diverging triangular end piece. A similar triangular piece is used at the distal end of the channel to collect the sample. As shown in Figure 1, the sample particles take different paths to reach the base of the triangular section. The particles traveling through the center of the channel will travel a shorter distance as compared to particles near the outside walls. These different flow paths are depicted by the dotted flow streamlines in Figure 1. This mismatch in the flow path length causes spreading of the sample along the length of the channel, a curved band, and band broadening as measured at a detector.[7,8] This spreading of the sample originating from the triangular ends is termed *end effects* in field-flow fractionation literature. Flow analysis using a conformal mapping technique showed progres-

* Corresponding author. Phone: (801) 585-3176. Fax (801) 585-9826. E-mail: himanshu.sant@utah.edu.

† E-mail: jungwootah.kim@samsung.com. Phone: +82-31-277-8058. Fax: +82-31-200-4872.

‡ E-mail: gale@eng.utah.edu. Phone: (801) 585-5944. Fax: (801) 585-9826.

(1) Giddings, J. C. *Sep. Sci.* **1966,** 1, 123−125.

(2) Gale, B. K.; Caldwell, K. D.; Frazier, A. B. *IEEE Trans. Biomed. Eng.* **1998**, *45*, 1459.

(3) Lao, A.; Trau, D.; Hsing, I. *Anal. Chem.* **2002,** *74*, 5364.

(4) Edwards, T.; Gale, B.; Frazier, A. *Anal. Chem.* **2002**, 1211.

(5) Yang, J.; Huang, Y.; Wang, X-B.; Becker, F.; Gascoyne, R. *Anal. Chem.* **1999**, *71*, 911.

(6) Kang, D.; Moon, M. *Anal. Chem.* **2004**, *76*, 3851−3855.

(7) Giddings, J.; Schure, R.; Myers, M.; Velez, G. *Anal. Chem.* **1984**, *56*, 2099−2104.

(8) Williams, P. S.; Giddings, S. B.; Giddings, J. C. *Anal. Chem.* **1986**, *56*, 2397−2403.

10.1021/ac0610154 CCC: $33.50
Published on Web 10/19/2006

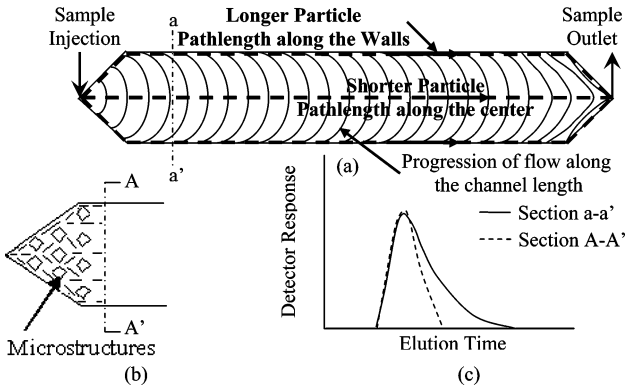

Figure 1. (a) Top view of the conventional FFF channel showing band broadening due to mismatch in pariticle pathlengths.[8] (b) Microstructures in the end triangular segments with improved flow profile due to redistribution of the streamlines. (c) Sharp particle elution profile with the use of microstructures at a section A−A′ compared to a conventional FFF channel with downstream section a−a′.

sively widening bands along the length of the channel that originate due to the presence of the inlet end piece. Band broadening further increases as the flow lines converge together at the outlet triangular end.[8]

Several recommendations have been made in the literature to help reduce these end effects. While describing the end effects in FFF for the first time, Giddings proposed reducing the volume of the ends as one method to reduce end effect-associated band broadening.[7] The spreading angle for the end pieces in FFF was also explored.[8] The requirement of a smooth transition from point injection to the bulk of the FFF channel favors the use of 60−90° as the inlet angle of the triangular end piece. None of these techniques completely eliminates the end effects, and from a manufacturing perspective, this reduced volume approach can be challenging and may result in sealing problems and a nonuniform field distribution.

In this paper, a new approach for reducing sample peak broadening and zone dispersion originating from the triangular ends is proposed to minimize instrument-related plate height, a critical performance parameter for field-flow fractionation and other separation systems. This improvement is especially important for microscale FFF systems in which instrumental plate heights can dominate and limit the resolution of the system.[9]

To further reduce end effects in FFF, we propose the use of microstructures in the channel ends to make all flow paths equal in length, which should reduce the band broadening associated with the triangular end pieces from the broad, curved sample band to a relatively flat profile, as shown in Figure 1. A variety of microstructures, essentially 3-D columns with different shapes and sizes, are incorporated in microscale FFF system ends. We first proposed this idea in earlier communications,[10,11] after which a similar approach was used to improve the detection in an FFF microsystem[12] and induce filtration in nanochannels.[13] The microstructures discussed here will redistribute the flow streams in the end piece and guide the particles to different flow paths such that the time delay between the particles reaching the rectangular section will be a minimum, as shown by the flow stream paths at the section A−A′ in Figure 1b. Essentially, the presence of microstructures in the end piece forces all paths to have similar lengths and fluid velocities, greatly reducing the dispersion associated with the end pieces. The reduction in the volume of the end pieces due to the presence of microstructures also reduces the overall retention time for a given flow rate in the channel, and thus, related time-based dispersion is also reduced. Because the analytical solution to the flow field for the triangular section with the microstructure column is complicated, we have used numerical analysis to solve for the velocity profile and particle dispersion associated with the addition of the microstructures in the end pieces. The simulations are geared toward obtaining an optimized shape, size, and location of the microstructures. The use of microstructures allows a reduction in the end effects while maintaining the conventional injection scheme and overall instrument design. Additionally, the use of a simple manufacturing technique first disseminated by our group[14] and expanded by our collaborators[15] can be extended to both microscale and macroscale FFF systems so that similar FFF channels can be fabricated without the need for special microfabrication facilities.

THEORY

Sample band broadening in field-flow fractionation is a combination of several factors, such as nonequilibrium (H_n), longitudinal diffusion (H_d), sample relaxation (H_r), sample polydispersity (H_p), sample volume (H_s), and instrumental effects (H_i).[16] These factors can be classified into two groups on the basis of their origin. The first group belongs to effects that give rise to Fickian diffusion-based dispersion. Contributions due to nonequilibrium plate height and longitudinal or axial diffusion fall into this category. The second category encompasses all other band-broadening factors that include sample and instrument-related effects. Sample relaxation, injection volume, polydispersity, and instrument-related plate height are included in this second category. Overall band broadening can be formulated as

$$H = H_d + H_n + H_r + H_p + H_i + H_s \qquad (1)$$

Over the last 20 years, instrument-related plate height has been ignored during FFF system optimization, since it was thought that little could be done to the channel itself. In addition, instrumental band broadening is generally not associated with operating conditions in FFF, so it cannot be minimized except by a redesign of an instrument, which can be an expensive and laborious process. A recent communication[9] from our lab has reported that

(9) Sant, H.; Gale, B. *J. Chromatogr., A* **2006**, *1104*, 282−290.
(10) Kim, J. W.; Sant, H.; Gale, B. Reduction of Microfluidic End Effects In Micro-Field Flow Fractionation Channels. In *Proc. MicroTAS 2003*; Squaw Valley, CA; October 5−9, 2003.
(11) Rao, S.; Sant, H.; Gale, B. Minimization of End Effects in Field Flow Fractionation. In *Proc. 10th Int. Symp. Field-Flow Fractionation*; Amsterdam, Netherlands; July 2−5, 2002.
(12) Blom, M.; Chmela, E.; Oosterbroek, E.; Tijssen, R.; Van Den Berg, A. *Anal. Chem.* **2003**, *75*, 6761−6768.
(13) Pennathur, S.; Santiago, J. *Anal. Chem.* **2005**, *77*, 6782−6789.
(14) Sant, H.; Gale, B. *Proc SPIE,* The *Int. Soc. Opt. Eng.*; vol. 5345; **2004**, 250−257.
(15) Bartholomeusz, D.; Bouté, R.; Andrade; *J. Microelectromech. Syst.* **2005**, *14*, 1364−1374.
(16) Schimpf, M.; Caldwell, K.; Giddings, J. *Field-Flow Fractionation Handbook*; Wiley-Interscience: New York; 2000, p 66.

instrumental effects can be very important, and it was shown that instrumental plate height is an important factor in total band broadening and resolution estimates, especially for microscale FFF channels.

Instrumental plate height takes into account the dispersion effects due to imperfect channel manufacturing and connection schemes. Instrumental plate height can actually be divided into three different categories: (i) factors related to the fractionation channel, which include design, geometry, integrity, quality of the channel surface, and roughness of the edges; (ii) factors related to the sample, which include reversible adsorption of the sample due to interaction with the channel surface; and (iii) factors related to extracolumn volumes, which includes precolumn and postcolumn volumes, sample injection method, and the detector flow cell volume-to-channel volume ratio. Band broadening due to the presence of the triangle ends falls into the first category and, in principle, can be minimized with proper modifications to the channel design.

As described previously, the mismatch in the analyte path length traveling straight through the center and along the edges of the triangle end results in analyte dispersion across the width of the channel and the so-called end effects in FFF. Quantitatively, for an open FFF channel, the plate height contribution due to the triangular ends (H_e) is given as

$$H_e = \frac{\tan^2\left(\frac{\theta}{2}\right) b^2 \beta^2}{4L} \tag{2}$$

where b is the channel width, θ is the inlet angle of the triangular end, β is the scaling parameter for the angle, and L is the length of the channel.[7,8,16]

On the basis of eq 2, one method for minimizing end effects would be to minimize θ, b, or both. Unfortunately, this approach in a traditional FFF channel causes edge effects to become more significant in generating dispersion and eliminates the infinite parallel plate geometry critical to successful FFF implementation. But the introduction of microstructures into the FFF channel end piece essentially implements this technique by implementing multiple, parallel, small θ paths radiating from a central injection point to minimize the plate height associated with getting the sample to the main FFF channel. The important question then to answer is whether the increase in edge effects (from increased particle retardation and perturbations due to the channel edges) overcomes the reduction in end effects. This question has been answered through the simulations and experiments that follow.

METHODOLOGY

Evidence for showing that the inclusion of microstructures in a FFF channel end piece can reduce plate heights was demonstrated using three methods: First, flow simulations for various end-piece configurations were performed to determine flow velocities and streamlines through the end pieces and to optimize the uniformity of the time required by particles to exit the end pieces. Second, using the results from the flow simulations, particle dispersion simulations through the end pieces to account for combined diffusion and advection effects were performed. Third, microscale FFF channels both with and without microstructures in the end pieces were manufactured, and the plate heights in the systems were measured.

Flow Simulation and Visualization. Particle-tracking simulations were used to visualize streamlines through the end pieces and were carried out by solving the velocity field numerically using Fluent 6.1 (Fluent Inc., NH) for a variety of FFF channel end-piece configurations. The three-dimensional geometry drawing was performed using ProEngineer (PTC, MA) and exported to GAMBIT for meshing. Unsteady, laminar flow was assumed for the flow simulations in Fluent. Pressure boundary conditions were used at the inlet and outlet with no-slip conditions at the walls of the channel section. Particles used in this simulation were weightless 100-nm-diameter spheres introduced across the inlet plane of the channel. The particles were tracked over time to determine streamlines in the flow and indicate the relative dispersion of particles due only to path length differences and convection effects.

Geometry Optimization. A plethora of the microstructures and the arrangements were simulated to obtain the best combination of microstructure column size, shape, and channel inlet angle. Channel inlet angles of 60° or 90° were used with either rhomboid or cylindrical microstructures of 100 and 200 μm located in the end pieces as appropriate. Spacing between the microstructures ranged from 50 to 200 μm. An adjustment to the placement of the microstructures was performed on the basis of the simulation results of the preliminary column arrangements. Figure 2 shows a schematic of an example of the type of the geometries used for the simulation. The dark shapes in the figure represent the microfluidic channel and input port, whereas the microstructures are depicted by the white shapes. The channel geometry for all flow simulations was 2 mm wide and 25 μm thick.

Particle Dispersion Analysis. Once an apparently optimum geometry was determined using flow modeling, numerical analysis of particle dispersion in the end piece of an FFF channel was done using COMSOL multiphysics software (COMSOL Inc., MA) to assess the effect of convective and Fickian diffusion on band broadening associated with the addition of microstructures to the FFF end piece, information that cannot be obtained just from the streamline visualization. The equations that govern particle transport in a field-flow fractionation system in the absence of any external field are the Navier−Stokes equation coupled to the convection−diffusion equation. For a constant-pressure driving force, the velocity field in an FFF channel can be specified by solving the stationary, nonlinear, laminar Navier−Stokes equation for an incompressible, isothermal, and Newtonian fluid. The momentum equation is solved to compute the velocity field and allow particle tracking.

There are two basic modes of mass transport in this case: diffusion and convection. For such a situation, the convection−diffusion equation for mass transport without a reaction term is

$$\frac{\partial C_j}{\partial t} = \nabla(D_j \nabla C_j - C_j U) \tag{3}$$

where $\partial/\partial t$ is the time derivative, j is the species index, D is the isotropic diffusion coefficient of the analyte, U is the velocity vector, and C is the concentration of the analyte. This time-dependent, mass-conservation equation is solved numerically to

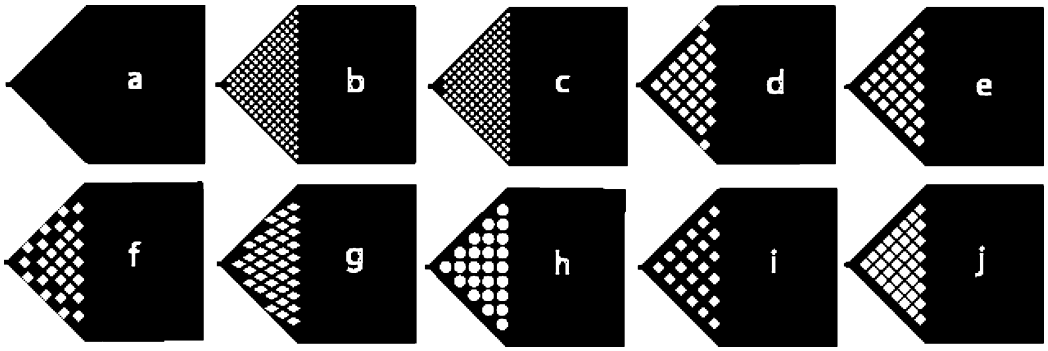

Figure 2. Schematic of the various microstructure designs for an example channel with a width of 4 mm. The example geometries are (a) without microstructures, (b) 100-μm circular microstructures spaced at 100 μm, (c) 100-μm square microstructures spaced at 100 μm, (d) 200-μm square microstructures spaced at 100 μm with additional columns at the end of the triangular section, (e) 200-μm square microstructures spaced at 100 μm, (f) 200-μm square microstructures spaced at 100 μm with additional columns at the edges of the triangular section, (g) 200-μm rhombus spaced at 100 μm with additional columns at the edges of the triangular section, (h) 200-μm circular microstructures spaced at 100 μm, (i) 200-μm square microstructures spaced at 200 μm, and (j) 200-μm square microstructures spaced at 50 μm.

compute particle dispersion in the FFF channel and provide an estimate of band broadening.

To enhance the end effects for better comparison, the channel for particle dispersion simulations and experiments was scaled 10 times in comparison to typical FFF geometrical dimensions as previously reported by Giddings.[7] The simulated channel is 3.5 cm long, 2 cm wide, and 25 μm thick with a 90° inlet angle. The presence of a symmetrical geometry allowed us to simulate only the one-fourth of the entire end piece providing efficient computation. For the numerical analysis, first a 2-dimensional top view of the section was drawn and meshed with 950 elements. This mesh was extruded to 12.5 μm, half the channel thickness, with 10 mesh layers in the *z* direction. This technique allowed us to efficiently mesh the entire 3-dimensional geometry with 46 750 mesh elements.

Once the mesh was set up and the boundary conditions were applied, the Navier−Stokes equations were solved to obtain the velocity field distribution in the channel section. Incompressible water with a density of 1000 kg/m^3 and viscosity of 0.001 N S/m^2 was used as the carrier solution. The boundary conditions used were (i) pressure at the inlet and outlet, (ii) no-slip at the microstructure and channel walls, and (iii) symmetry on the other sides. A stationary nonlinear UMFPAK solver was used to solve for the velocity field and pressure distribution in the channel. This velocity field distribution was stored and used for solving the convection diffusion equation to obtain the transient particle concentration profile in the channel.

Like any chromatography system, field-flow fractionation requires introduction of an impulse injection of the sample at the start of the experimental run with a continuous carrier flow in background. To mimic this situation, an additional rectangular section (50 μm long) was used at the inlet, thus dividing the geometry into two subdomains. To solve the convection-diffusion equation, the sample injection domain was loaded with an initial concentration of a particle sample with diffusion coefficient of 2.8 $\times$ 10^{-12} m^2/s. The boundary conditions were (i) zero concentration at the inlet of the sample injection domain, (ii) convective flux at the outlet of the channel domain, (iii) continuity at the interface, and (iv) insulation or symmetry at either side. A nonlinear, transient GMERS solver was used with a 0.01-s time step to solve the convection−diffusion equation until the bulk of the injected sample had moved out of the simulated end piece.

Prototype Device Fabrication. The prototype device for comparison to the numerical simulations was manufactured on a polished glass substrate using microfabrication techniques. First, input and output ports of 1/16" diameter were drilled using a Dremel tool on an optically flat thin glass slide (Fisher Scientific, NH). This was followed by sputter-deposition of 1000 Å of titanium and 3000 Å of gold. The metal layers were photolithographically patterned to yield a 100-μm-wide electrode wire using a positive photoresist mask and an iodine-based etch with a weight-based composition of potassium iodide (Fisher Scientific, NH), iodine (Fisher Scientific, NH), and DI water (4:1:4) to etch the gold and a 1% hydrofluoric acid solution to etch the titanium. The metal structures served as an AC impedance electrode for sample detection. The electrode wires proceed to a bond pad area at the end of the glass slide. Photoresist SU-8 (25 μm thick, Microchem, MA) was used to define the channel walls and microstructures in the triangular end section using standard photolithography. The photomask was designed in such a way that it allowed us to realize both the microchannel and microstructures in a single step. An identical electrode was patterned on another glass substrate, and both glass substrates were bonded together using a UV-curable adhesive to realize a parallel plate field-flow fractionation channel. A thin adhesive trough was provided around the channel while patterning the SU-8 to allow a perfect seal between the two glass substrates without any adhesive's wicking into the channel and destroying the flow pattern. A similar device without any microstructures was fabricated using the same procedures for comparison. The fabrication process for the SU-8 channel wall and metal electrode patterning is explained in more detail in other papers.[14]

Packaging and Experimental Setup. All the fluidic connectors, including tubing, ferrules, nuts, and a t-injector, were purchased from Upchurch Scientific, WA. At the inlet port of the system, a 1/16-in. ferrule was glued as a guide to the 1/16-in.-o.d. and 0.030-in.-i.d. PEEK tubing. A t-injector was connected to this PEEK tube to enable us to inject sample and flow carrier solution simultaneously, as shown in Figure 3. A syringe pump

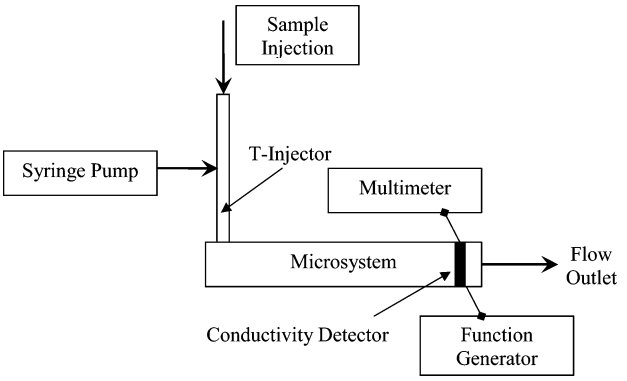

Figure 3. Schematic diagram of the assembly of the experimental setup. Flow system through the microsystem and electrical connections for the on-chip conductivity detector can be seen.

(Kent Scientific, CT) with a 3-mL gastight syringe (Hamilton, NV) delivered a constant flow of carrier to the microchannel through one end of the t-injector through 1/16-in. Teflon tubing, and a sample was injected using a microliter syringe (Hamilton, NV) through the third opening of the t-injector. Backflow from this opening was prevented by using a membrane ferrule. The outlet of the channel was kept open to the atmosphere, and the eluted carrier was allowed to flow into a waste collection reservoir located outside the prototype system.

The metal electrode wires were used as an impedance-based particle detection scheme. A signal generator was used to supply the 2 VPP AC voltage at a frequency of 10 kHz to the impedance electrodes. A multimeter was connected in series with the detector and signal generator, as shown in the Figure 3, to record the current. Continuous data collection was performed using Labview software on a PC through a GPIB card connected to the multimeter.

Plate Height Measurement. Plate height measurement for both dispersion and experimental studies was based on properties of the sample elution peak. Number of plates, N, can be calculated from the measured values of half peak width, $w_{1/2}$, and elution volume of the peak, A, as

$$N = 5.54\left(\frac{A}{w_{1/2}}\right)^2 \tag{4}$$

Using plate theory, plate height can be calculated by dividing the length of the channel by the number of plates as

$$H = \frac{L}{N} \tag{5}$$

Chemicals. Polystyrene particles of 200-nm diameter (Bangs Labs, Fishers, IN) without any surface modification were used for the plate height measurements. Ultrafiltered DI water (Barnstead Corporation, IA) was used as the carrier solution.

Safety Considerations. The hydrofluoric acid used to etch the titanium electrodes is a highly corrosive chemical, and proper safety precautions with acid protective gloves and aprons should be taken while using it. UV-protective glass should be used during photolithography and UV light-induced adhesive curing process.

RESULTS AND DISCUSSION

Fabrication and Packaging Results. The channel height for the microscale prototype was measured as 25 μm using a profilometer (Tencor, CA) before bonding. The prototype used for the experimental verification of plate height was found to have well-developed microstructures without any distortions. The channel height of the packaged system was checked under an optical microscope by focusing first the planar SU-8 on the glass slide and then on the edge of the glass underneath. By recording the distance traveled by the microscope stage between the two focusing steps, the channel height of the packaged prototype was measured and found to be 25 $\pm$ 0.2 μm. Flow testing of the prototype showed no leaks or unwanted flow disturbances.

Particle Tracking Analysis. Our goal of using microstructures is to reduce plate height, which is a direct measure of the band broadening in field-flow fractionation. We have measured this plate height just outside the triangular section, and for this reason, any improvement in plate height should be the direct result of the incorporation of the microstructures.

The numerical simulation of the time-dependent position of the injected sample particles in the channel demonstrated that compact particle bands could be obtained with the inclusion of microstructures in the triangular ends when compared to open end pieces. Figure 4 shows the results of two simulations for direct visual comparison and clearly shows that the addition of microstructures to the end piece produces a much more compact sample band with greatly reduced dispersion along the length of the channel. Figure 4a shows how the open end pieces produce a highly curved sample band in the main section of the FFF channel. Although the particles are well-distributed across the width of the microchannel, they are also distributed across a significant length of the channel. When microstructures are included in the triangular ends, a tighter particle distribution is obtained with a nearly flat particle band across the width of the channel (Figure 4b). A typical detector observing particles leaving the end piece in this situation would indicate a relatively sharp peak, as compared to a rather broad peak for the situation n which no microstructures are included.

The simulation results in Figure 5b indicate some of the issues associated with including microstructures in the channel end piece. First, "edge" effects become more significant because the particles in the end piece have much more surface to negotiate, and the structure approximating infinite parallel plates is disrupted. The simulation indicates, though, that the amplified edge effects do not overcome the improvement associated with equalizing the streamline lengths. Second, the inclusion of square structures or rhomboidal structures essentially creates multiple small end effects, resulting in small bumps and local stretching in the particle band exiting the triangular end pieces. Both of these effects should be minimized by choosing an appropriate geometry. Thus, a number of experiments and simulations were performed to optimize the microstructure column location and geometry to obtain a better sample distribution and to minimize local edge effects.

Geometry Optimization. For quantitative comparison of the particle dispersion due to the variety of microstructures and spacing used in the simulations, we measured the time-dependent position of an array of particles using the particle tracking function

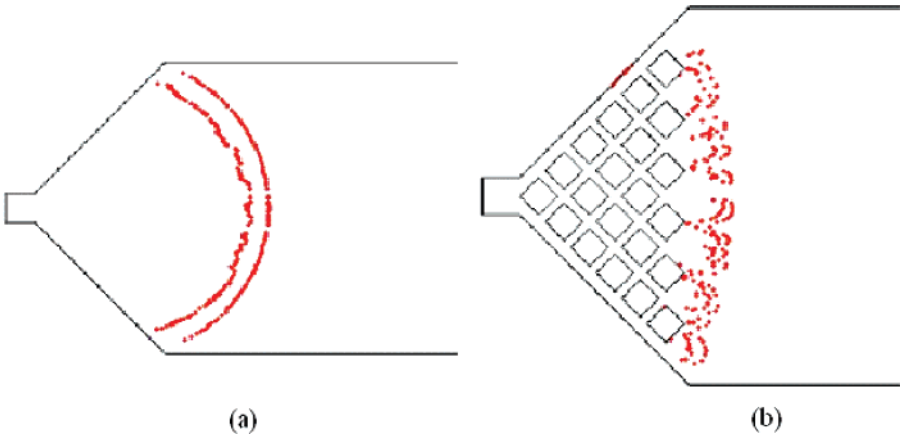

Figure 4. Particle trace snapshot at a distance of 17 mm from the injection edge. Channel dimensions are 3.5 mm × 2 mm × 100 μm. The average flow velocity used was 1.5 mm/s in the main section of the channel. The end piece in part b uses 200-μm square microstructures.

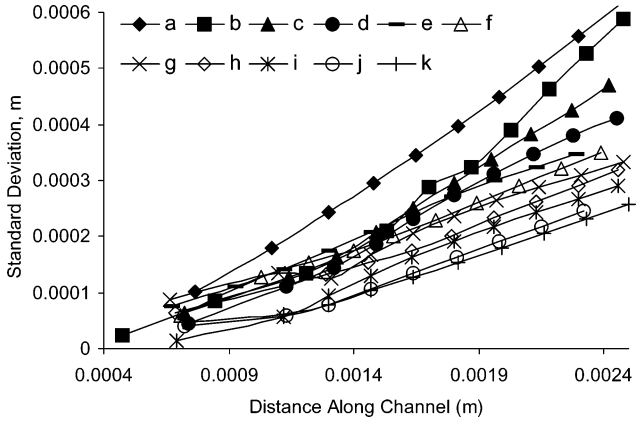

Figure 5. Plots of the standard deviation of the distance traveled by the particles as a function of the distance the particles have traveled: (a) without microstructures, (b) 60° inlet angle with 100-μm circular microstructures at 100-μm spacing, (c) 60° inlet angle with 100-μm square microstructures at 100-μm spacing, (d) 60° inlet angle with 100-μm square microstructures at 100-μm spacing and first microstructure column removed, (e) 90° inlet angle with 100-μm square microstructures at 100-μm spacing and first microstructure removed, (f) 90° inlet angle with 200-μm rhombus spaced at 100 μm with additional microstructures at the edges of the triangular section, (g) 90° inlet angle with 100-μm square microstructures at 25-μm spacing and first microstructure removed, (h) 90° inlet angle with 200-μm circular microstructures spaced at 100 μm, (i) 90° inlet angle with 200-μm square microstructures spaced at 50 μm with additional microstructures at the edges of the triangular section, (j) 90° inlet angle with 200-μm square microstructures spaced at 100 μm with additional microstructures at the edges of the triangular section, and (k) 90° inlet angle with 200-μm square microstructures spaced at 200 μm with additional microstructures at the edges of the triangular section.

in Fluent. The position of the injected sample particles along the length of the channel for different time instances was recorded, and the mean and the standard deviation of the particle position along the FFF channel were calculated from these data. Figure 5 is the compilation of the calculated standard deviation of the particle positions along the length of the channel as a function of average distance traveled by a particle down the channel for a variety of microstructure geometries and configurations in the end pieces. The arrangement of microstructures shown in Figure 2e was found to have the least dispersion among all the structures simulated. There are 28 microstructures of 200-μm squares spaced at 100 μm in this design. This arrangement is one of the simplest and satisfies the requirement of equal pathlengths across the width of the FFF channel. Path length along the walls of the channel is visibly reduced with an open passage without any restrictions. In contrast, along the center of the channel, flow lines diverge and converge several times around the microstructures before reaching the open channel at the end of the end piece. It should be noted that FFF channels have a high aspect ratio, and in general, the path length and the time required to traverse the end piece are directly related. The beauty of the presented system is that it forces all paths to have similar lengths and fluid velocities, greatly reducing the dispersion associated with the end pieces. If the presence of the microstructures results in a mismatch of pathlengths during the flow redistribution, a wider elution profile compared to the open channel may result.

A few observations on the data are also of interest. For some microstructure configurations, removing the very first microstructure near the sample inlet helped direct flow into the bulk of the end piece instead of along the far edges. In addition, the data indicated that the distance between the walls of the channel and the microstructures was important for the same reason. If all spaces were the same, the flow along the outside edges was faster than the flow through the central channels, leading to increased particle dispersion. Thus, it is recommended that the spacing between microstructures be twice that of the spacing between the walls and the structures to eliminate this difference and even out flow rates.

Particle Dispersion Analysis. Although streamline path visualization and particle tracking gives a good estimate of the dispersion of the sample particles due only to advection, it does not take into account effects such as diffusion. A complete particle dispersion analysis using COMSOL multiphysics software was performed to analyze the dispersion of polystyrene particles under more general experimental conditions and for more common channel thicknesses.

Figure 6 shows a simulated detector output based on the particle dispersion simulations. Figure 6a is an elution peak for a conventional open-channel FFF design, whereas Figure 6b is a FFF channel with microstructures in the inlet triangular end. Clearly, with microstructures, band broadening is reduced, and a tighter particle band can be obtained. The simulation shown in

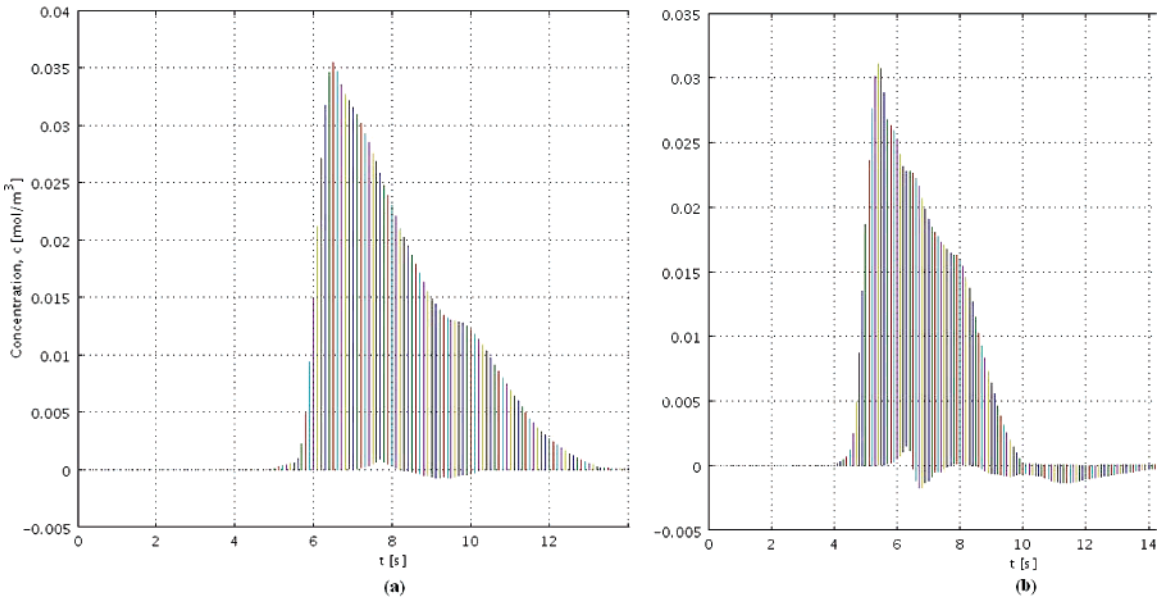

Figure 6. Typical particle elution peaks at the exit edge of the channel. The dimensions of quarter section of the channel are 3.5-mm length × 1-mm width × 12.5-μm thickness. A scaled version of microstructures from Figure 2e are used for the simulation. The flow velocity during this simulation is 1.5 mm/s, and particle diffusion coefficient is 2.8×10^{-12} m^2/s.

Figure 6 suggests more peak tailing for the channel with microstructures. We believe this effect arises due to the small edge effects observed in Figure 4. As the particles travel along the edges of the microstructures, some particles are retarded and result in local stretching of the bands. The overall effect of this local stretching is increased peak tailing for the channel with microstructures. This effect should be reduced with optimization of the microstructure geometry and locations. The elution profile shown in Figure 6 is generated 17 mm downstream of the end piece. The particle band just outside the end piece would be more compact, and the effect of the microstructures would be more visible, but the detector was placed in this position to match the experimental conditions. Thus, better results than these might be possible.

One of the reasons to carry out the simulations shown in Figure 6 was to determine if there are any steric effects on the particle distribution due to the presence of the microstructures. It is anticipated that steric effects may become dominant as the size of the particles approaches the gap distance between the microstructures and results in sluggish flow and unwanted particle retardation. The simulations did not reveal any local steric effects due to the microstructures and provided a generally improved particle elution profile, as illustrated in Figure 7. It should be noted that the particle sizes analyzed using the microscale FFF channel were well below 1 μm, and with 100-μm microstructure spacing, the flow of both the carrier and the particles should be smooth.

An important benefit of particle dispersion analysis is that it provides a direct measure of the plate height for the system. Plate height data can be directly compared with the other microsystems for a quantitative comparison. Figure 7 shows just such a calculation from the particle dispersion simulations. Plate heights from the particle dispersion analysis were measured according to the procedure described in the experimental section. Figure 7 shows that the plate height can be reduced with the inclusion of the microstructures by as much as 1/3, thus further validating

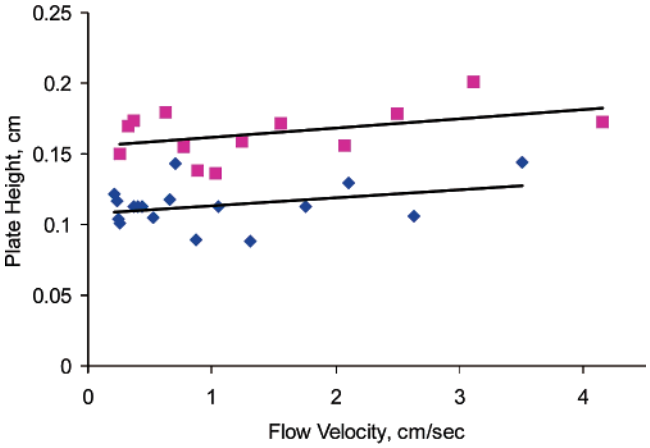

Figure 7. Plate height comparison using particle dispersion simulations. ■ denotes trace of plate height data for conventional open channel FFF system. ♦ denotes trace of plate height data for FFF channel with microstructure columns in the ends.

the hypotheses of using microstructures to reduce band broadening.

Experimental Plate Height Measurements. The experimental plate height for a channel with the best column arrangement, as determined by the simulations, was measured and compared to the results from a conventional FFF microchannel without structures, as shown in Figure 8. Figure 8 shows the results of these plate height measurements at a series of flow rates for both the open and structure-filled end pieces. Linear fits to the data indicate the trends in the plate height variation with the flow rate, a standard technique to represent band-broadening data in FFF.[17] Generally, the instrumental contribution of plate height, H_i, is measured by the extrapolated intercept on the plate height axis of a graph of plate height as a function of carrier flow rate. For a microsystem, the plate height measurements shown in

(17) Gale, B. K.; Caldwell, K. D.; Frazier, A. B. *Anal. Chem.* **2002**, *74*, 1024–1030.

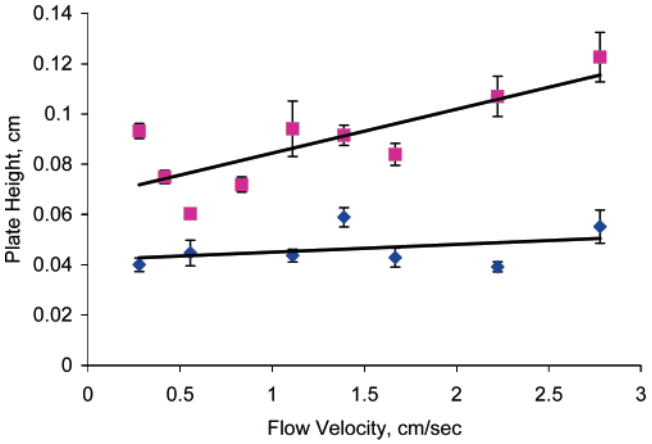

Figure 8. Plate height measurements for the prototypes with and without microstructure columns. ■ denotes plate height data for the conventional open-channel FFF system. ♦ denotes trace of plate height data for FFF channel with microstructure columns in the ends.

Figure 8 are relatively high, but it should be remembered that a wider than usual channel was used to maximize end effects for better comparison. It is clear from these experiments and the simulations that the use of microstructures results in an average 50% improvement in the instrumental plate height.

An inadvertent advantage associated with the inclusion of microstructures in the end pieces is that the total retention time for a given particle actually falls for a given volume flow rate through the channel. This reduction in time occurs because the total volume of the end pieces is significantly less than for the standard end pieces, so the particles move more quickly through the end pieces, and the total time is reduced. For the end pieces used here, this time reduction can be up to 5% of the total retention time and leads to faster analysis while improving the separation quality.

CONCLUSIONS

The redistribution of path lengths using easy-to-manufacture microstructures was shown as an efficient way to reduce band broadening in FFF channels. Particle path lines and particle dispersion analysis were used to optimize the size, shape, and structure of the microstructures in the triangular end pieces. Structures (200-μm square) spaced at 100-μm intervals resulted in the best flow profile among the variety of structures and shapes used in this study. Local edge effects due to the presence of the microstructures that may limit how compact a particle band can be obtained were observed. Experimental plate height measurement was shown to follow the trends predicted by the numerical models and simulations. An average 50% reduction in plate height was achieved with modified channel end pieces. The addition of microstructures to the end pieces allows higher peak capacities and could prove to be a critical factor in the performance of microscale FFF systems designed for achieving faster separations of multicomponent samples. Further study should involve the effect of scaling these microstructures, and efforts should be made to optimize the microstructures according to the channel thickness. Such a method to better distribute the sample in a microchannel can be used to improve the sample injection systems and performance of other microfluidic devices that rely on similar geometries.

ACKNOWLEDGMENT

This work was supported by the Department of Mechanical Engineering and Technology Innovation Grant at the University of Utah. The authors thank Dr. Henry White and Dr. Mark Miller for assistance with the flow simulations.

Received for review June 2, 2006. Accepted September 15, 2006.

AC0610154